Study of ^{249}Bk, ^{241}Am, and ^{231}Pa with proton transfer reactions*

J. R. Erskine
University of Minnesota, Minneapolis, Minnesota 55455
and Argonne National Laboratory, Argonne, Illinois 60439

G. Kyle
University of Minnesota, Minneapolis, Minnesota 55455

R. R. Chasman and A. M. Friedman
Argonne National Laboratory, Argonne, Illinois 60439

(Received 26 August 1974)

Proton single-particle states have been studied in the isotopes ^{249}Bk, ^{241}Am, and ^{231}Pa. The reaction (α, t) was utilized in the three studies. Additionally, the reaction $(^3\mathrm{He}, d)$ was used in the study of levels in ^{249}Bk. Many new levels were observed and some could be interpreted in terms of single-particle orbitals. Also several assignments previously made on the basis of radioactive decay studies were confirmed by the orbital signatures seen in the proton transfer spectra. Single-particle energies are extracted from the experimental data. Deformations of the nuclear central potential are deduced for ^{249}Bk and ^{241}Am. By use of the parameters of the central field for ^{249}Bk, the $f_{7/2}$-$f_{5/2}$ splitting is deduced for mass 250 at zero deformation and estimated for mass 300.

[NUCLEAR REACTIONS ^{248}Cm(^{3}He, d), ^{248}Cm, ^{240}Pu, ^{230}Th(α, t) E=29 MeV; measured E (excitation), σ; deduced orbitals, s.p. energies, deformations in ^{249}Bk, ^{241}Am, ^{231}Pa.]

I. INTRODUCTION

The knowledge of proton single-particle excitations in the actinide region is quite limited. Most of this information comes from radioactive decay studies. The use of single-proton transfer reactions affords an opportunity to increase this fund of information considerably. The single-proton transfer reaction is a powerful tool for the unambiguous identification of single-proton states, particularly when the orbital of interest is populated in several of its rotational states. In this work we present a study of proton states as determined by proton transfer reaction studies throughout the actinide region. We have studied levels in a nuclide representing the light actinides, ^{231}Pa; the mid-actinide region, ^{241}Am; and the heavy actinides, ^{249}Bk. The reactions employed in our study, (α, t) and $(^3\mathrm{He}, d)$, provide information only on particle states. Sufficient energy for the $(d, ^3\mathrm{He})$ reaction leading to hole states is not available to us for high resolution studies at this time.

It has been suggested[1] that the use of the $(^3\mathrm{He}, d)$ and (α, t) reactions facilitates the assignment of l values to observed transitions. According to distorted-wave–Born-approximation (DWBA) calculations, the decrease in cross section with increasing angular momentum is about twice as steep in the $(^3\mathrm{He}, d)$ reaction as it is in the (α, t) reaction. By taking ratios of cross sections, one should have a fairly sensitive method for determining the orbital angular momentum of levels populated in these studies. One of our purposes is to test this approach.

In Sec. II, we give a brief discussion of the theoretical framework used in our analysis. We present figures showing the energies of actinide proton orbitals as a function of various deformation multipoles. We also give a table of wave function component intensities, $C_j{}^2$. In Sec. III, we present our experimental procedures and in Sec. IV, our experimental results. In Sec. V, we discuss the single-particle orbital assignment of levels and relate them to the underlying single-particle model. In this same section we also discuss the values of our absolute cross sections and $(\alpha, t)/(^3\mathrm{He}, d)$ cross-section ratios in terms of theoretical calculations. Preliminary results of this study have been reported earlier.[2,3]

II. THEORETICAL ANALYSIS

The theoretical framework used for the analysis of our single-proton transfer data is similar to that used previously for our single-neutron transfer data.[4] To make the present discussion self-contained, the major features will be sketched. The basic approximation is that the differential

cross section can be factored into two parts: θ_J^{DW} depending on the reaction mechanism and S_J^α depending on the nuclear eigenstates. In the case of an even-even target nucleus, this approximation is

$$\frac{d\sigma_J^\alpha}{d\Omega} = (2J+1)\theta_J^{\mathrm{DW}} S_J^\alpha \ , \tag{1}$$

where J is the total spin and α signifies the other quantum numbers of the single-particle state being populated. We computed the single-particle transfer cross section θ_J^{DW} for the (α, t) and $(^3\mathrm{He}, d)$ reactions using the DWBA code DWUCK.[5] The spectroscopic factor S_J^K is calculated for the nuclear Hamiltonian

$$H = H_{\text{single particle}} + H_{\text{pairing}} \ . \tag{2}$$

Each of the two terms in the nuclear Hamiltonian affects the magnitude of the spectroscopic factor S_J^α. The single-particle wave functions in the deformed field are generated from $H_{\text{single particle}}$. The deformed wave functions, written in terms of a spherical basis, are

$$\psi_\alpha = \sum_J C_J^\alpha \Phi_J \ , \tag{3}$$

where Φ_J is a spherical eigenfunction. The spectroscopic factor for the rotational level based on the single-particle state ψ_α and having spin J is proportional to the square of the expansion coefficient $(C_J^\alpha)^2$. Pairing forces influence the spectroscopic factor in that they determine the occupation probability of the various single-particle states in the initial and final systems. From the single-particle and pairing terms in our Hamiltonian, we obtain the following expression for the spectroscopic factor.

$$S_J^\alpha = [2/(2J+1)]\,(C_J^\alpha)^2[1 - \langle N_\alpha(A-1)\rangle] \ , \tag{4}$$

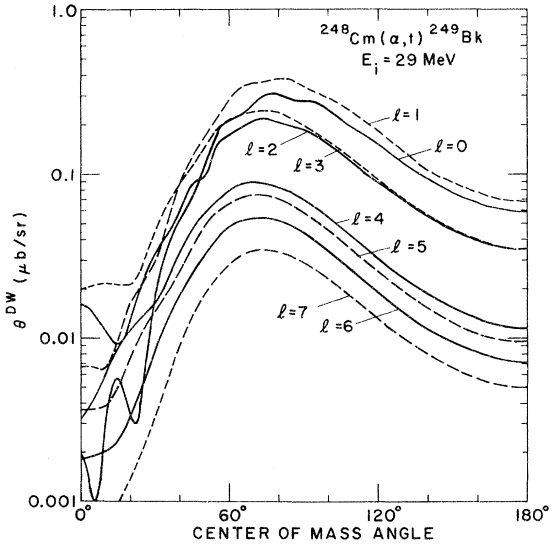

FIG. 1. Calculated angular distributions for the $^{248}\mathrm{Cm}(\alpha, t)^{249}\mathrm{Bk}$ reaction to the ground state at 29-MeV bombarding energy.

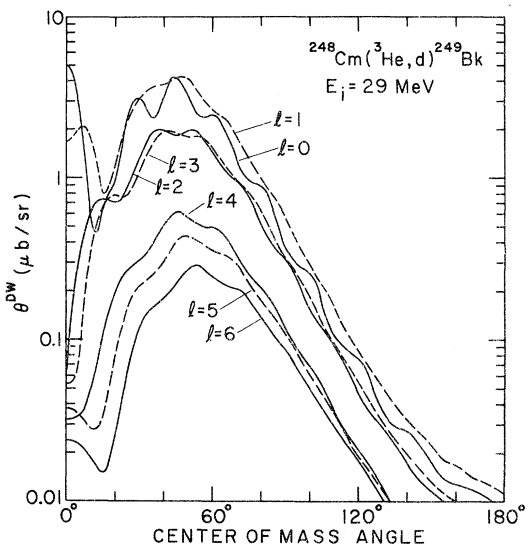

FIG. 2. Calculated angular distributions for the $^{248}\mathrm{Cm}(^3\mathrm{He}, d)^{249}\mathrm{Bk}$ reaction to the ground state at 29-MeV bombarding energy.

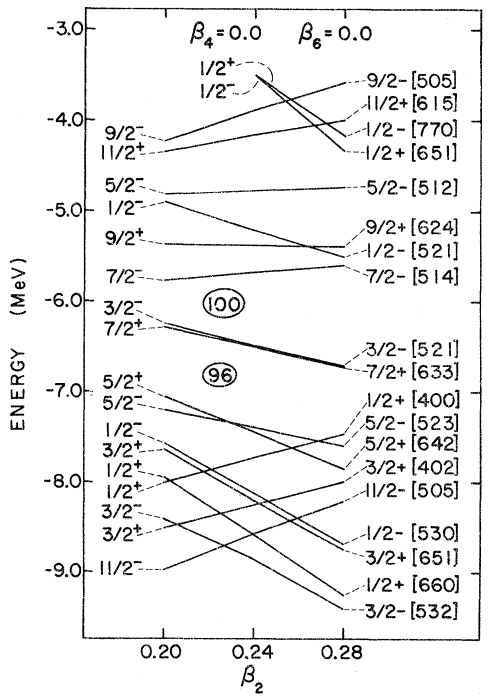

FIG. 3. Energies of actinide proton orbitals as a function of β_2 ($\beta_4 = 0, \beta_6 = 0$).

where $\langle N_\alpha(A-1)\rangle$ is the occupation probability of the state ψ_α in the ground state of the nucleus having mass $A-1$. This spectroscopic factor is modified[6] when Coriolis mixing is important.

The DWBA calculations were carried out with the computer code DWUCK .[5] The optical-model parameters used are those given by Elze and Huizenga.[1] The calculations assumed the zero-range approximation and no radial cutoff. Zero-range normalization factors used were $N=4.42$ for (^{3}He, d) reactions and $N=46$ for (α, t) reactions. Computed angular distributions for $l=0$ to 7 for the reaction ^{248}Cm(α, t)^{249}Bk are shown in Fig. 1 and for the reaction ^{248}Cm(^{3}He, d)^{249}Bk in Fig. 2.

We have calculated deformed single-particle wave function and their energies using a momentum dependent Woods-Saxon potential previously[7] described. In Fig. 3, we display the dependence of the single-particle energy on quadrupole deformations. In Fig. 4, we display the hexadecapole deformation dependence of these energies and in Fig. 5 the dependence on β_6 deformations. We have varied these deformations over the ranges expected to occur for actinide nuclides. The deformations are introduced into the potential through the substitution

$$r^2 \to r^2[\sin^2\theta e^{2\beta_2/3} + \cos^2\theta e^{-4\beta_2/3} + \beta_4 P_4^0(\cos\theta) + \beta_6 P_6^0(\cos\theta)] \ .$$

We have fixed the magnitude of the spin-orbit potential by making the orbitals $\frac{3}{2}$−[521] and $\frac{7}{2}$+[633] degenerate. The spacing between these orbitals is quite insensitive to changes of β_2, β_4, or β_6 over the ranges shown in Figs. 3–5 and serves as a convenient way to fix the spin-orbit potential. In Table I, we list the values of $C_J{}^2$ for the actinide proton orbitals. Note that the $\frac{1}{2}$+[651] labeling is somewhat anomalous, but we have not changed it to avoid confusion.

III. EXPERIMENTAL PROCEDURE

29-MeV beams of ^{3}He and α particles from the University of Minnesota model MP tandem Van de Graaff accelerator were used in these experiments. The reaction products were analyzed with an Enge split-pole magnetic spectrograph.[8] The solid angle used was about 3.1 ms. Nuclear track plates (Kodak type NTB 50 μm) were used to record the data that were later hand scanned. Foils of cellulose triacetate were found necessary to eliminate unwanted background tracks in both the (α, t) and (^{3}He, d) spectra. The energy resolution width for the spectra was 18–25 keV.

Two silicon monitor counters, located at ±30°

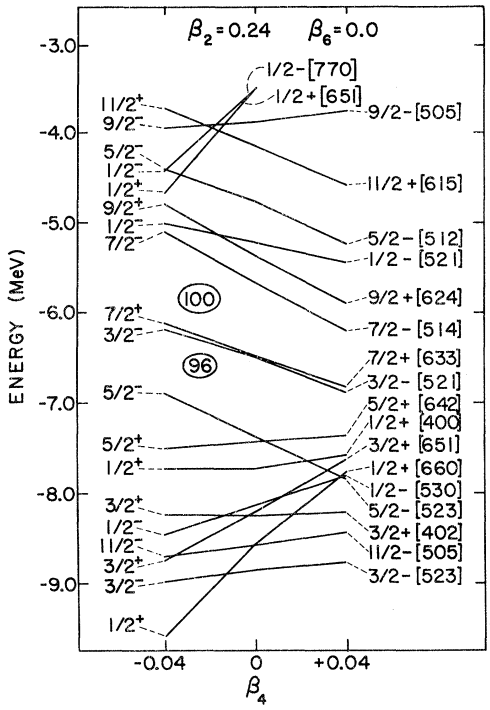

FIG. 4. Energies of actinide proton orbitals as a function of β_4 ($\beta_2=0.24$, $\beta_6=0$).

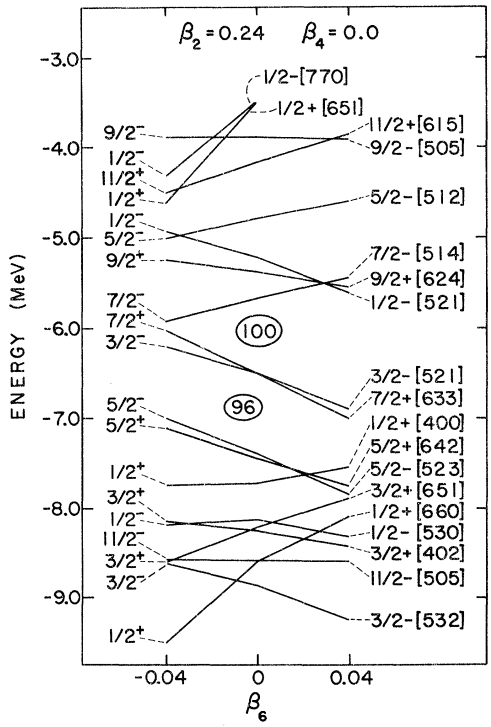

FIG. 5. Energies of actinide proton orbitals as a function of β_6 ($\beta_2=0.24$, $\beta_4=0$).

TABLE I. Deformed single-particle wave functions for the actinide proton orbitals. The values of C_J^2 and a which were calculated in a momentum-dependent Woods-Saxon potential are given. The table was calculated with deformation parameters $\beta_2 = 0.24$, $\beta_4 = 0.0$, and $\beta_6 = 0.0$.

Orbital	$\langle S_Z + \frac{1}{2} \rangle$ [a]	$C_{1/2}^2$	$C_{3/2}^2$	$C_{5/2}^2$	$C_{7/2}^2$	$C_{9/2}^2$	$C_{11/2}^2$	$C_{13/2}^2$	$C_{15/2}^2$	a
$\frac{1}{2}$+[651]	0.65	0.044	0.083	0.156	0.200	0.142	0.308	0.065	0.000	−0.99
$\frac{1}{2}$−[770]	0.55	0.000	0.001	0.000	0.017	0.000	0.151	0.000	0.810	−7.70
$\frac{9}{2}$−[505]	0.05					0.993	0.006	0.000	0.000	
$\frac{11}{2}$+[615]	0.95						0.003	0.993	0.000	
$\frac{5}{2}$−[512]	0.94			0.016	0.876	0.055	0.053	0.000	0.000	
$\frac{1}{2}$−[521]	0.22	0.254	0.030	0.322	0.197	0.173	0.023	0.000	0.000	1.08
$\frac{9}{2}$+[624]	0.89					0.017	0.005	0.972	0.000	
$\frac{7}{2}$−[514]	0.11				0.019	0.964	0.015	0.001	0.000	
$\frac{3}{2}$−[521]	0.87		0.110	0.013	0.693	0.091	0.093	0.000	0.000	
$\frac{7}{2}$+[633]	0.83				0.000	0.049	0.005	0.938	0.000	
$\frac{5}{2}$−[523]	0.19			0.051	0.028	0.896	0.024	0.001	0.000	
$\frac{5}{2}$+[642]	0.76			0.002	0.001	0.089	0.005	0.895	0.000	
$\frac{1}{2}$+[400]	0.98	0.682	0.183	0.113	0.017	0.005	0.000	0.000	0.000	0.58
$\frac{1}{2}$−[530]	0.80	0.034	0.290	0.001	0.432	0.124	0.120	0.000	0.000	−2.39
$\frac{3}{2}$+[651]	0.68		0.000	0.008	0.001	0.128	0.003	0.851	0.000	
$\frac{3}{2}$+[402]	0.04		0.877	0.073	0.046	0.004	0.000	0.000	0.000	
$\frac{1}{2}$+[660]	0.57	0.001	0.000	0.015	0.000	0.154	0.000	0.819	0.000	6.63
$\frac{11}{2}$−[505]	1.00						0.991	0.000	0.001	
$\frac{3}{2}$−[532]	0.29		0.011	0.145	0.028	0.786	0.028	0.001	0.000	

[a] S_Z is the expectation value of the Z component of the spin operator. $\langle S_Z + \frac{1}{2} \rangle$ is the probability of finding spin up in the wave function. $\langle S_Z + \frac{1}{2} \rangle = 1$ for pure spin-up states, and $\langle S_Z + \frac{1}{2} \rangle = 0$ for pure spin-down states.

with respect to the beam, were used to determine the absolute differential cross section. The spectrograph was used to record a short exposure of the beam elastically scattered from the target. The elastic scattering cross section at 30° was assumed to be pure Coulomb scattering, as indicated by optical-model calculations. The absolute cross sections for the long reaction exposures (10 000 to 20 000 μC) could then be calculated from the ratio of the monitor counts during the long and short runs.

The (α, t) exposures were taken at 80° observation angle since this was at a maximum in the angular distribution. A few spectra were recorded at 45°, but these were of less value due to the smaller cross sections at this angle. All (^{3}He, d) spectra were taken at 60° observation angle. The spectra were analyzed with the automatic spectrum decomposition program AUTOFIT.[9] In most spectra the ground-state transition was not observed. In these cases excitation energies were found relative to assumed energies of levels previously known from decay scheme studies.

The targets for this study were prepared by J. Lerner with the Argonne experimental isotope separator. The isotopes in the beam from the separator were deposited directly onto a self-supporting carbon backing. The target material (typically 50 to 100 μg/cm^2 in thickness) was generally confined to a rectangular area 1 ⊗ 3 mm. The line shape of the target reduced the background in the spectra as well as the total amount of radioactivity present on the target. The latter was useful for reasons of safety.

IV. EXPERIMENTAL RESULTS

The spectra obtained with the (^{3}He, d) and (α, t) reactions populating levels in ^{249}Bk are shown in

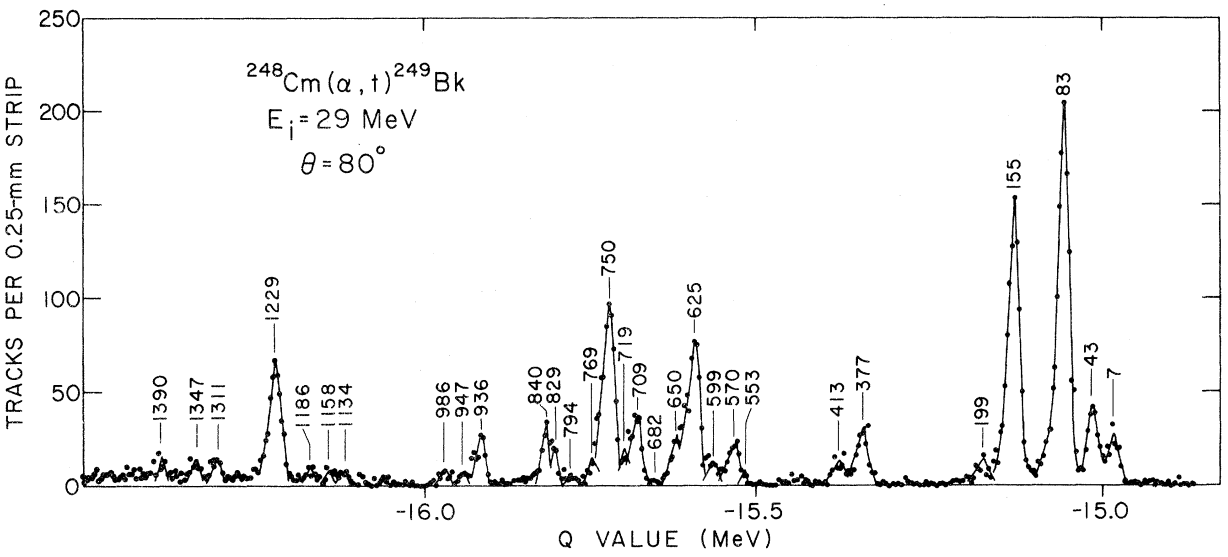

FIG. 6. Triton spectrum from the ^{248}Cm$(\alpha,t)^{249}$Bk reaction observed at 80°. Levels in ^{249}Bk are labeled by their excitation energy in keV.

Figs. 6 and 7. Spectra from the (α, t) reaction leading to ^{241}Am and ^{231}Pa are shown in Figs. 8 and 9. Tables II–IV list the excitation energies, measured absolute differential cross sections, and assignments made to the levels (to be discussed below). For the level in ^{249}Bk the cross section ratio $d\sigma(\alpha, t)/d\sigma(^3\text{He}, d)$ appears in Table II as this quantity was used as an aid in making some of the assignments.

V. DISCUSSION

A. Level assignments in ^{249}Bk

Our investigation of ^{249}Bk is the most extensive of the three nuclei studied, since we were able to obtain good spectra for both the ^{248}Cm$(\alpha, t)^{249}$Bk and the ^{248}Cm$(^3\text{He}, d)^{249}$Bk reactions. An energy level diagram of ^{249}Bk which includes all assign-

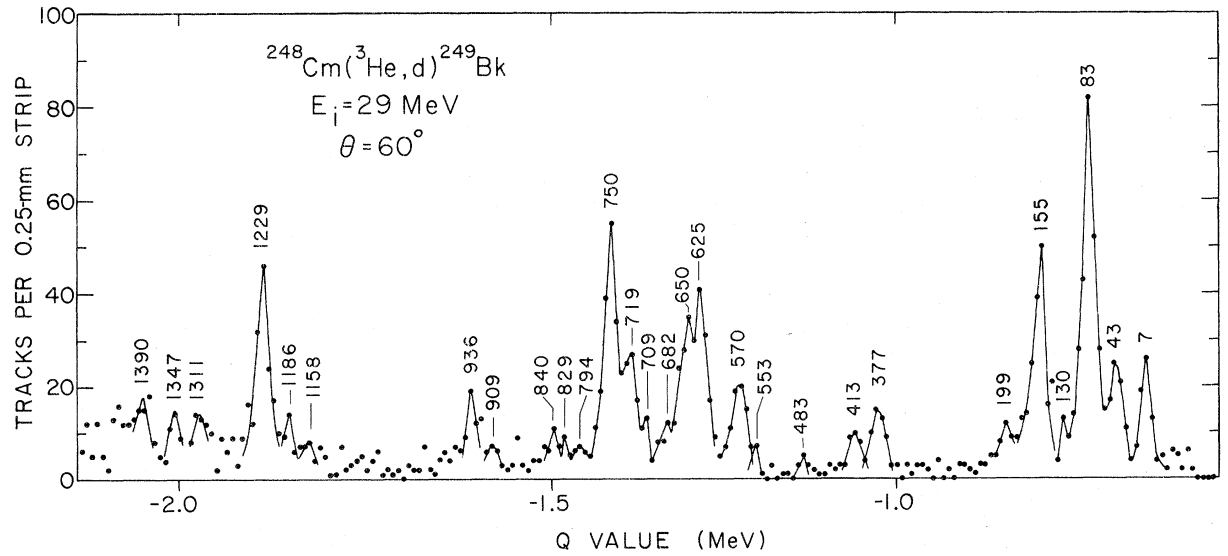

FIG. 7. Deuteron spectrum from the ^{248}Cm$(^3\text{He}, d)^{249}$Bk reaction observed at 60°. Levels in ^{249}Bk are labeled by their excitation energy in keV.

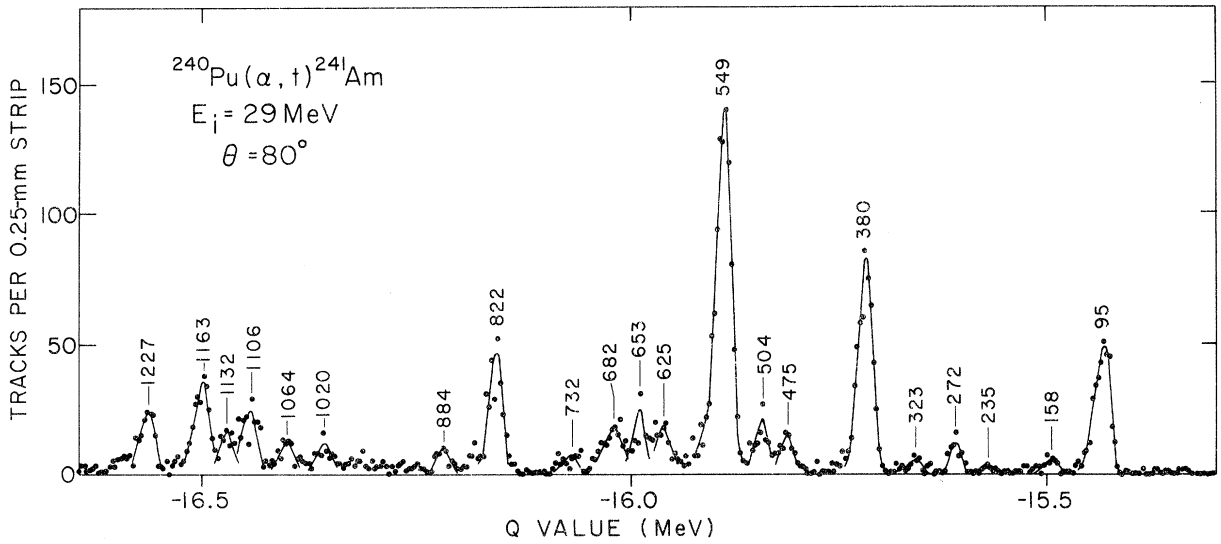

FIG. 8. Triton spectrum from the ^{240}Pu$(\alpha,t)^{241}$Am reaction observed at 80°. Levels in ^{241}Am are labeled by their excitation energy in keV.

ments made from the present study as well as for decay studies[10] is presented in Fig. 10.

1. $\frac{7}{2}$+[633], $\frac{3}{2}$−[521], and $\frac{5}{2}$+[642]

Three rotational bands, built on the orbitals $\frac{7}{2}$+[633], $\frac{3}{2}$−[521], and $\frac{5}{2}$+[642] have been identified in ^{249}Bk from α-decay studies[10] of ^{253}Es.

A large transfer cross section is expected for transitions to the $I^\pi=\frac{7}{2}^-$ member of the $\frac{3}{2}$−[521] band. We see this large cross-section transition at 83 keV as well as smaller cross sections for transitions to the $I^\pi=\frac{3}{2}^-$, $\frac{5}{2}^-$, $\frac{9}{2}^-$, and $\frac{11}{2}^-$ members of this rotational band. A large cross section is also expected for the population of the $I^\pi=\frac{13}{2}^+$ member of the $\frac{7}{2}$+[633] band at 155 keV. We see a large cross section here. The transfer data are in full agreement with the assignments of the orbitals $\frac{7}{2}$+[633] and $\frac{3}{2}$−[521].

Since the $\frac{5}{2}$+[642] orbital is a hole state in ^{249}Bk, it is not strongly populated in our transfer studies. Further, the $I^\pi=\frac{13}{2}^+$ is the only member of the rotational band with a large $C_j{}^2$. We see a weak transition to a level at 599 ± 4 keV which is con-

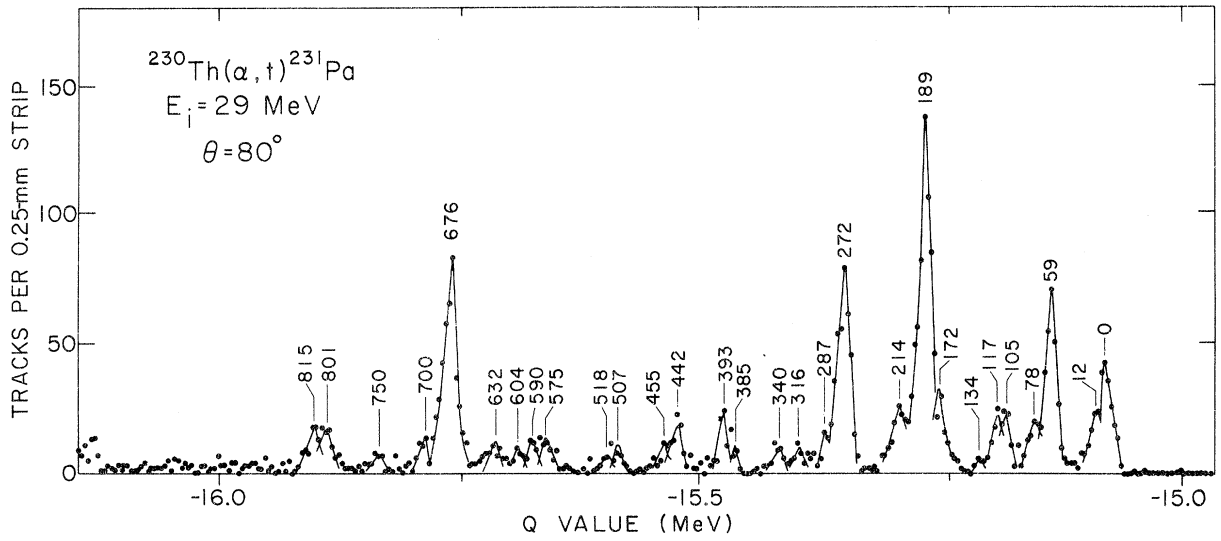

FIG. 9. Triton spectrum from the ^{230}Th$(\alpha,t)^{231}$Pa reaction observed at 80°. Levels in ^{231}Pa are labeled by their excitation energy in keV.

TABLE II. Energy levels in ^{249}Bk, their excitation energies, their differential cross sections observed with the (α,t) and $(^3\mathrm{He},d)$ reactions, and their orbital assignments.

Level No.	Excitation energy (keV)	$d\sigma(\alpha,t)/d\Omega$ [a] 80° (μb/sr)	$d\sigma(^3\mathrm{He},d)/d\Omega$ [a] 60° (μb/sr)	Ratio= $\frac{d\sigma(\alpha,t)}{d\sigma(^3\mathrm{He},d)}$	Assignment of level I	Orbital	Confidence [b]
1	7 ± 3	9.8 ± 1	4.3 ± 0.7	2.3 ± 0.44	$\frac{3}{2}$	$\frac{3}{2}$−[521]	A
2	43 ± 3 [c]	14.1 ± 1.5	5.1 ± 0.7	2.8 ± 0.49	$\frac{9}{2}$	$\frac{7}{2}$+[633]	A
					$\frac{5}{2}$	$\frac{3}{2}$−[521]	A
3	83 [d]	70.7 ± 4	15.5 ± 1.2	4.6 ± 0.44	$\frac{7}{2}$	$\frac{3}{2}$−[521]	A
4	130 ± 3	<4	1.8 ± 0.6		$\frac{9}{2}$	$\frac{3}{2}$−[521]	A
5	155 ± 1	53.3 ± 3	9.6 ± 0.8	5.6 ± 0.56	$\frac{13}{2}$	$\frac{7}{2}$+[633]	A
6	199 ± 3	4.4 ± 1	2.3 ± 0.8	1.9 ± 0.79	$\frac{11}{2}$	$\frac{3}{2}$−[521]	A
7	377 ± 2	10.7 ± 0.8	2.9 ± 0.4	3.7 ± 0.58	$\frac{1}{2}$	$\frac{1}{2}$+[400]	C
8	413 ± 2	4.7 ± 0.7	1.5 ± 0.3	3.1 ± 0.77	$\frac{3}{2}$, $\frac{5}{2}$	$\frac{1}{2}$+[400]	C
9	483 ± 5	<2	0.3 ± 0.2		$\frac{9}{2}$	$\frac{5}{2}$+[642]	C
10	553 ± 6	2.0 ± 1	1.0 ± 0.8	2.0 ± 1.89	$\frac{1}{2}$		C
11	570 ± 3	8.2 ± 0.7	4.0 ± 0.6	2.1 ± 0.36	$\frac{3}{2}$		C
12	599 ± 4	4.3 ± 0.6	<1		$\frac{13}{2}$	$\frac{5}{2}$+[642]	B
13	625 ± 1	26.9 ± 1.5	8.3 ± 0.9	3.2 ± 0.39	$\frac{9}{2}$	$\frac{5}{2}$−[523]	C
14	650 ± 5 [c]	8.3 ± 2	5.4 ± 0.6	1.5 ± 0.40			
15	682 ± 6	0.5 ± 0.4	1.0 ± 0.5	2.0 ± 3	$\frac{11}{2}$	$\frac{5}{2}$−[523]	C
16	709 ± 5	12.9 ± 0.8	1.0 ± 0.6				
17	719 ± 4	2.0 ± 0.9	6.0 ± 1.5				
18	750 ± 1	34.4 ± 1.5	10.0 ± 0.8	3.4 ± 0.31	$\frac{9}{2}$	$\frac{7}{2}$−[514]	C
19	769 ± 5	3.9 ± 0.7	<0.8				
20	794 ± 5	1.3 ± 0.5	0.9 ± 0.6	1.1 ± 0.85			
21	829 ± 3	3.2 ± 1.0	0.5 ± 0.4	6.4 ± 5.50	$\frac{11}{2}$	$\frac{7}{2}$−[514]	C
22	840 ± 3	7.9 ± 1.0	1.3 ± 0.6	6.1 ± 2.92			
23	909 ± 5	<1	0.8 ± 0.4				
24	936 ± 4	8.3 ± 1.0	3.9	2.1			
25	947 ± 10	1.0 ± 0.6	1.0 ± 0.6	1.0 ± 0.85			
26	986 ± 8	1.7	<0.5				
27	1134 ± 8	1.7	<0.5				
28	1158 ± 6	1.1	1.0	1.0			
29	1186 ± 8	1.7	2.0	0.9			
30	1229 ± 2	24 ± 1.5	8.5 ± 0.8	2.8 ± 0.32	$\frac{13}{2}$	$\frac{9}{2}$+[624]	C
31	1311 ± 5	3.8 ± 0.8	2.9 ± 0.7	1.3 ± 0.42			
32	1347 ± 7	3.1 ± 0.8	2.5 ± 0.6	1.2 ± 0.42			
33	1390 ± 6	3.8 ± 0.8	2.4 ± 0.6	1.6 ± 0.52			

[a] The relative uncertainties are given in the table. These numbers taken as absolute differential cross sections have an additional uncertainty of about 20%.

[b] Confidence levels A, B, and C mean that the indicated assignments are well-established, probable, and plausible, respectively.

[c] Unresolved doublet.

[d] Reference state whose excitation energy is assumed to be 83 keV.

TABLE III. Energy levels in ^{241}Am, their excitation energies, their different cross sections observed with the (α,t) reaction, and their orbital assignments.

Level No.	Excitation energy (keV)	$d\sigma(\alpha,t)/d\Omega$ [a] 80° (μb/sr)	I	Assignment of level Orbital	Confidence [b]
1	95 [c]	20 ±1.5	$\frac{9}{2}$	$\frac{5}{2}$−[523]	A
2	158±2	2.2±0.3	$\frac{11}{2}$	$\frac{5}{2}$−[523]	A
3	235±5	1.0±0.6	$\frac{7}{2}$	$\frac{5}{2}$+[642]	A
4	272±2	4.2±0.6	$\frac{9}{2}$	$\frac{5}{2}$+[642]	A
5	323±4	2.1±0.4	$\frac{11}{2}$	$\frac{5}{2}$+[642]	A
6	380±1	30.8±1.5	$\frac{13}{2}$	$\frac{5}{2}$+[642]	A
7	475±4	5.2±0.7	$\frac{3}{2}$	$\frac{3}{2}$−[521]	A
8	504±3	6.6±0.8	$\frac{5}{2}$	$\frac{3}{2}$−[521]	A
9	549±1	53.3±2.5	$\frac{7}{2}$	$\frac{3}{2}$−[521]	A
10	625±3	7.4±0.8	$\frac{1}{2}$	$\frac{1}{2}$+[400]	C
11	653±4	6.0±0.7	$\frac{3}{2}$, $\frac{5}{2}$	$\frac{1}{2}$+[400]	C
12	682±3	7.5±0.8	$\frac{11}{2}$	$\frac{3}{2}$−[521]	C
13	732±4	2.4±0.6	$\frac{11}{2}$	$\frac{7}{2}$+[633]	B
14	822±4	18.9±2.0	$\frac{13}{2}$	$\frac{7}{2}$+[633]	B
15	884±4	2.7±0.6			
16	1020±4	3.4±0.6			
17	1064±4	3.8±0.6			
18	1106±4	8.5±0.9			
19	1132±5	4.8±1.0			
20	1163±3	12.8±1.0	$\frac{9}{2}$	$\frac{7}{2}$−[514]	C
21	1227±3	8.9±0.9			

[a] The relative uncertainties are given in the table. These numbers taken as absolute differential cross sections have an additional uncertainty of about 20%.

[b] The confidence levels A, B, and C mean that the indicated assignments are well-established, probable, and plausible, respectively.

[c] Reference state show excitation energy is assumed to be 95 keV.

sistent with the $\frac{13}{2}^+$ level assigned at 598 keV in the α-decay studies.

2. $\frac{5}{2}$−[523] and $\frac{7}{2}$−[514]

The $\frac{5}{2}-[523]$ state is known in other actinide nuclei and should occur in ^{249}Bk as a hole state at an energy of about 500 keV. This state has a large Coriolis interaction matrix element (1.3) with the $\frac{7}{2}-[514]$ particle state also expected near 500 keV excitation. Their combined signatures calculated with the inclusion of Coriolis mixing show strong transitions to the $I=\frac{9}{2}$ levels and weaker ones to the $I=\frac{11}{2}$ levels. Levels 13 (625 keV) and 15 (682 keV) fit the predicted signature of the $I=\frac{9}{2}$ and $\frac{11}{2}$ levels of the $\frac{5}{2}-[523]$ band and levels 18 (750 keV) and 21 (829 keV) fit the signature of the $I=\frac{9}{2}$ and $\frac{11}{2}$ levels of the $\frac{7}{2}-[514]$ band when band mixing is taken into account. However, the Coriolis matrix elements had to be reduced to about 30% of their theoretical value. (See discussion to follow in Sec. V D.) Following the above assignment, the rotational constants for these bands are 5.2 and 7.2 keV with an average of 6.2 keV which is consistent with the value for this band in ^{241}Am and ^{231}Pa. The average rotational constant for the unmixed $\frac{5}{2}-[523]$ state is known to be 5.8 keV in ^{241}Am and 6.4 in ^{231}Pa. The $K=\frac{7}{2}$ state is assigned with degree of confidence C since its signature is so largely perturbed by Coriolis mixing. The assignment of the $K=\frac{5}{2}$ state is even more questionable.

3. $\frac{1}{2}$+[400]

Hoff *et al.*[11] have studied the β decay of ^{249}Cm and identified several low spin states in ^{249}Bk.

TABLE IV. Energy levels in ^{231}Pa, their excitation energies, their differential cross sections observed with the (α,t) reaction, and their orbital assignments.

Level No.	Excitation energy (keV)	$d\sigma(\alpha,t)/d\Omega$ [a] 80° (μb/sr)	Assignment of level I	Orbital	Confidence [b]
0	0	13.2 ± 1.1	$\frac{3}{2}$	$\frac{1}{2}$−[530]	A
1	12 ± 4	5.3 ± 1.0	$\frac{1}{2}$	$\frac{1}{2}$−[530]	A
2	59 ± 1	19.6 ± 1.2	$\frac{7}{2}$	$\frac{1}{2}$−[530]	A
3	78 ± 2	5.4 ± 0.8	$\frac{5}{2}$	$\frac{1}{2}$−[530]	A
4	105 ± 3	4.7 ± 0.9	$\frac{7}{2}$, $\frac{3}{2}$	$\frac{3}{2}$+[651]	B
5	117 ± 4	5.5 ± 0.9	$\frac{9}{2}$	$\frac{3}{2}$+[651]	B
6	134 ± 5	1.2 ± 0.6	$\frac{11}{2}$	$\frac{3}{2}$+[651]	B
7	172 ± 3	5.7 ± 2.1	$\frac{11}{2}$	$\frac{1}{2}$−[530]	B
8	189 ± 1	41.8 ± 4	$\frac{13}{2}$	$\frac{3}{2}$+[651]	B
9	214 ± 2	10.0 ± 2.2	$\frac{7}{2}$	$\frac{5}{2}$−[523]	A
10	272 ± 1	24.3 ± 1.5	$\frac{9}{2}$	$\frac{5}{2}$−[523]	A
11	287 ± 3	5.0 ± 0.8	$\frac{1}{2}$	$\frac{1}{2}$+[400]	B
12	316 ± 4	2.7 ± 0.7	$\frac{3}{2}$, $\frac{5}{2}$	$\frac{1}{2}$+[400]	B
13	340 ± 3	2.8 ± 0.8	$\frac{11}{2}$	$\frac{5}{2}$−[523]	B
14	385 ± 5	1.0 ± 0.5			
15	393 ± 2	7.5 ± 2.0			
16	442 ± 2	4.8 ± 0.5	$\frac{13}{2}$	$\frac{5}{2}$+[642]	
17	455 ± 2	2.4 ± 0.5			
18	507 ± 3	1.9 ± 0.4			
19	518 ± 3	0.8 ± 0.4			
20	575 ± 5	2.0 ± 0.5			
21	590 ± 5	2.0 ± 0.5			
22	604 ± 4	2.5 ± 0.7	$\frac{3}{2}$	$\frac{3}{2}$−[521]	C
23	632 ± 3	3.0 ± 0.8	$\frac{5}{2}$	$\frac{3}{2}$−[521]	C
24	676 ± 2	25.2 ± 3.1	$\frac{7}{2}$	$\frac{3}{2}$−[521]	C
25	700 ± 3	4.0 ± 1.6			
26	750 ± 2	1.7 ± 0.4			
27	801 ± 3	4.1 ± 0.5	$\frac{11}{2}$	$\frac{3}{2}$−[521]	C
28	815 ± 3	4.7 ± 0.5			

[a] The relative uncertainties are given in the table. These numbers taken as absolute differential cross sections have an additional uncertainty of 20%.

[b] Confidence levels A, B, and C mean that the indicated assignments are well-established, probable, and plausible, respectively.

One band they observed has positive parity; the $I=\frac{1}{2}$ level was 377.8 keV and $I=\frac{5}{2}$ level was at 421.4 keV. Our levels 7 (377 keV) and 8 (413 keV) could be the $I=\frac{1}{2}$ and $\frac{3}{2}$ levels of the same band. They also form a signature very similar to one that we observe for the $I=\frac{1}{2}$ and $\frac{3}{2}$ levels of the $K^{\pi}=\frac{1}{2}^{+}$ band in ^{241}Am.

In order to identify the particular orbital involved here, we have computed for the (α, t) reaction the signatures of the three most likely candidates for this state, $\frac{1}{2}$+[400], $\frac{1}{2}$+[660], and $\frac{1}{2}$+[651]. These three computed signatures are displayed in Fig. 11 together with the observed signature. The single-particle transfer cross

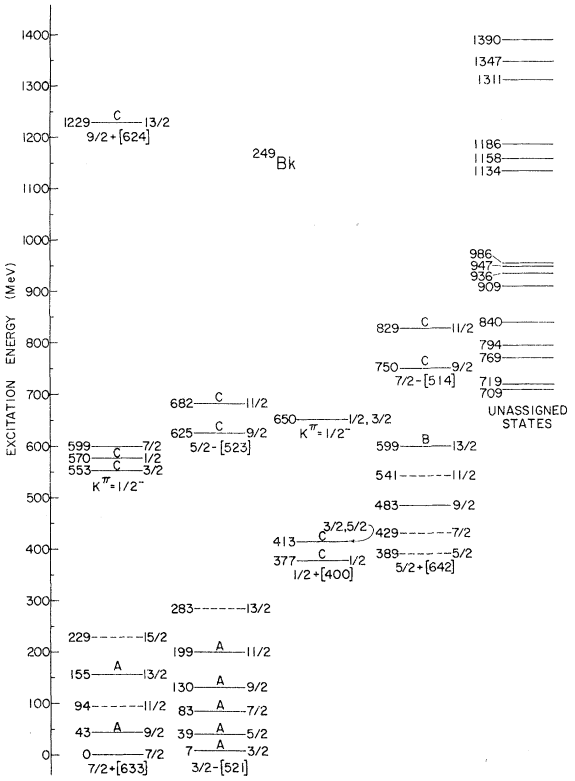

FIG. 10. Energy level diagram for ^{249}Bk. Wherever possible the levels have been assigned to rotational bands whose asymptotic quantum numbers are given below each band. The measured excitation energies (in keV) and assigned spins are given. The confidence level of each assignment is denoted by letters A (well-established), B (probable), and C (plausible). Dashed lines indicate levels seen in other studies but not in present work.

sections were calculated with the wave functions of Table I and the DWBA code described in Sec. II. As can be seen in the figure, the $\frac{1}{2}+[400]$ assignment is in far better agreement with the cross-section data than either the $\frac{1}{2}+[660]$ or $\frac{1}{2}+[651]$ assignments.

There is a difficulty with this assignment, however, and that is that the measured ration of (α, t) to (^{3}He, d) cross sections for the 377-keV level indicates that the transferred orbital angular momentum l is 4 ± 1, which is not consistent with a $\frac{1}{2}^+$ assignment. As will be discussed below in Sec. V E we believe this discrepancy is most likely due to some unknown peculiarity in the ratio technique, rather than a misassignment of the $\frac{1}{2}+[400]$ orbital.

4. $\frac{1}{2}-[530]$ and $\frac{1}{2}-[521]$

Hoff *et al.*,[11] on the basis of ^{249}Cm β-decay data report new $K^\pi=\frac{1}{2}^-$ rotational bands at 569.3 and 643.1 keV in ^{249}Bk. We have observed levels at 553 ± 6, 570 ± 3, and at 650 ± 5 keV having (α, t)/(^{3}He, d) cross-section ratios consistent with low l-value assignments, and hence consistent with the $\frac{1}{2}^-$ assignments of Hoff *et al.*

It is difficult to make single-particle orbital assignments for either of these $K^\pi=\frac{1}{2}^-$ rotational bands; the $\frac{1}{2}-[521]$ orbital is expected to be a somewhat higher particle state and the $\frac{1}{2}-[530]$ orbital is expected to be a deep hole state in the Bk isotopes. From our study of ^{231}Pa, we have an experimental signature for the orbital $\frac{1}{2}-[530]$ which consists of large cross sections to the $I^\pi=\frac{3}{2}^-$ and $\frac{7}{2}^-$ members of the rotational band with smaller cross sections to the $I^\pi=\frac{1}{2}^-$ and $\frac{5}{2}^-$ members. The signature of the $\frac{1}{2}-[521]$ orbital has not been observed experimentally, but it is expected to consist of observable peaks to the $I^\pi=\frac{1}{2}^-$, $\frac{5}{2}^-$ and the $I^\pi=\frac{7}{2}^-$, and $\frac{9}{2}^-$ doublet (assuming the calculated decoupling constant of $+1$).

If our low l-value transitions are assigned to members of either the $\frac{1}{2}-[530]$ or $\frac{1}{2}-[521]$ rotational bands then we see no evidence for the expected transitions to the second rotational level

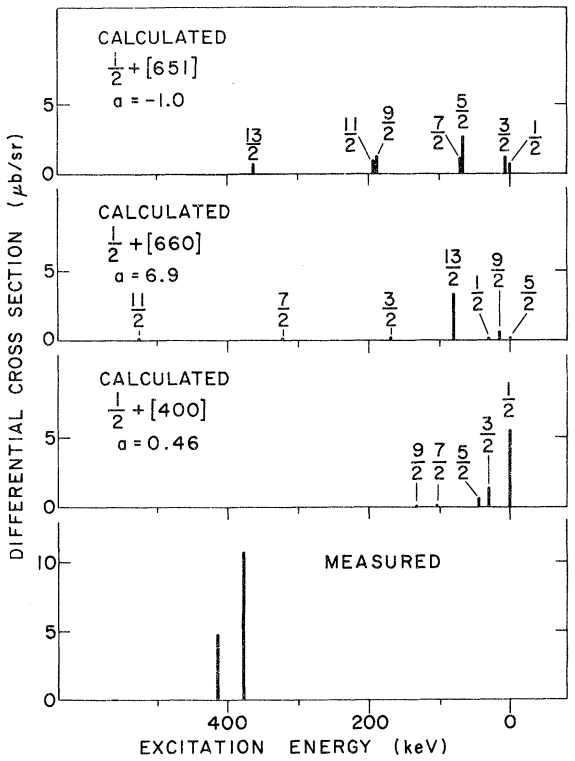

FIG. 11. Signatures of $\Omega^\pi=\frac{1}{2}^+$ states in ^{249}Bk. Theoretical signatures of the $\frac{1}{2}+[400]$, and $\frac{1}{2}+[660]$, and $\frac{1}{2}+[651]$ states for the ^{248}Cm$(\alpha, t)^{249}$Bk reaction are shown for comparison with the observed signature of the $\Omega^\pi=\frac{1}{2}^+$ state at 377 keV.

of each band (i.e., the $I^\pi = \frac{1}{2}^-$ level of the $\frac{1}{2}^-[530]$ band or $I^\pi = \frac{3}{2}^-$ or $\frac{5}{2}^-$ levels of the $\frac{1}{2}-[521]$ band). While the signatures could be changed by Coriolis mixing of these bands, our calculations indicate that band-mixing effects are not large.

Therefore, it appears that these $K^\pi = \frac{1}{2}^-$ bands are not simply the $\frac{1}{2}-[521]$ and $\frac{1}{2}-[530]$ states. We have recently made measurements of the ^{246}Cm$(\alpha, t)^{247}$Bk reaction which show very strong similarities to spectra of the ^{248}Cm$(\alpha, t)^{249}$Bk reaction between 0.5 and 1.0 MeV excitation. Final analysis of these new data may lead to a more complete understanding of the band structure in this region of excitation.

5. $\frac{9}{2}+[624]$

The particle state $\frac{9}{2}+[624]$ is expected to lie near 1 MeV excitation on the basis of deformed shell-model calculations. The theoretical signature of this state suggests that only the $I^\pi = \frac{13}{2}^+$ level of the band will be observed. The strongly excited level that we observe at 1229 ± 2 keV has a $(\alpha, t)/(^3\text{He}, d)$ cross-section ratio of 2.8 which indicates high spin. Therefore, we assign the 1229 level as the $\frac{13}{2}^+$ member of the $\frac{9}{2}+[624]$ rotational band, with confidence level C.

B. Level assignments in ^{241}Am

Many levels in this nucleus have been identified in the studies of both the α decay of ^{245}Bk (Ref. 12) and the electron capture decay of ^{241}Cm by Porter *et al.*[12] We see transitions to many of these same states and confirm these assignments. An energy level diagram of ^{241}Am which contains our present assignments together with other assignments made on the basis of decay data[13] is given in Fig. 12.

1. $\frac{5}{2}^-[523]$

The $I = \frac{5}{2}$, $\frac{7}{2}$, and $\frac{9}{2}$ levels of this band were identified in Ref. 12 as being at 0, 41.17, and 93.4 keV which indicates a rotational constant of 5.85 keV for this band. This leads to a predicted energy of 157.8 keV for the $I = \frac{11}{2}$ level of the band. Levels 1 and 2 at 95 and 158 ± 2 keV have the correct cross sections and energy spacing for the $I = \frac{9}{2}$ and $\frac{11}{2}$ levels and are assigned to them. The predicted cross sections for the transitions to the $I = \frac{5}{2}$ and $\frac{7}{2}$ levels are so small that we should not see them.

2. $\frac{5}{2}+[642]$

In Ref. 12 the $I = \frac{5}{2}$, $\frac{7}{2}$, $\frac{9}{2}$, $\frac{11}{2}$, and $\frac{13}{2}$ levels of this band were identified in the α decay of ^{245}Bk as being at 207, 234, 272, 322, and 380 keV, respectively. Our levels 3 (235 keV), 4 (272 keV), 5 (323 keV), and 6 (380 keV) fit the energies of the $I = \frac{7}{2}$, $\frac{9}{2}$, $\frac{11}{2}$, and $\frac{13}{2}$ levels of this band. However, the cross section for the population of these levels has presumably been increased by the Coriolis coupling with the $\frac{7}{2}+[633]$ orbital.

In addition to the Coriolis mixing there appears to be an additional perturbation of the signature of these states. Evidence for this effect is as follows: A study of Table I indicates that the values of C_j^2 for both the $I = \frac{7}{2}$ and $\frac{11}{2}$ levels of all the positive parity $N = 6$ bands are very small and therefore transitions to these levels should not be seen. Furthermore, the magnitude of these transitions will not be affected by Coriolis forces since the value of C_j^2 is small for all states involved. However, the observed cross sections for populating the $I = \frac{7}{2}$ and $\frac{11}{2}$ levels are about 50% of the cross sections for populating the $I = \frac{9}{2}$ level in ^{241}Am. The most likely explanation is that there are coupling effects in the reaction channel, perhaps Coulomb excitation in the target or residual nucleus, which shift some of the total transition amplitudes to other rotational states. Unfortunately, we have not had a suitable coupled channel transfer code to use in estimating the magnitude of this shift.

3. $\frac{3}{2}^-[521]$

The $I = \frac{3}{2}$, $\frac{5}{2}$, and $\frac{7}{2}$ levels of this band were identified in Refs. 12 and 13 as being at 472, 502, and

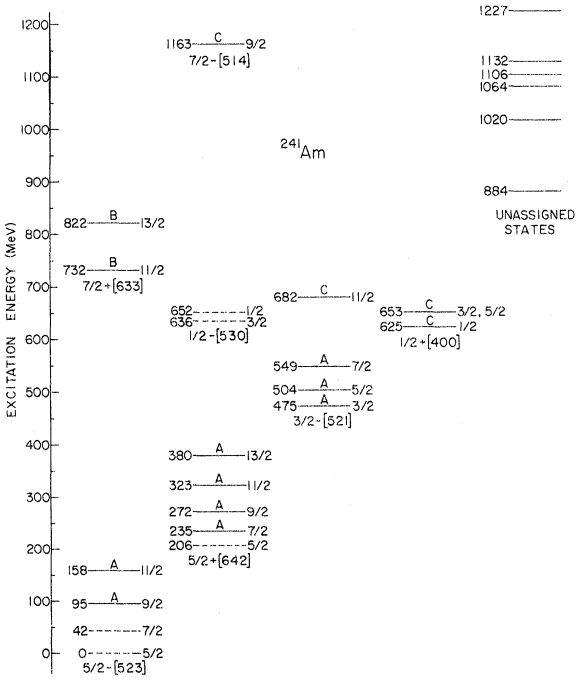

FIG. 12. Energy level diagram for ^{241}Am. See caption of Fig. 10 for further description.

549 keV, respectively, and populated in the unhindered α decay of ^{245}Bk. The energies of levels 7 (475 keV), 8 (504 keV), and 9 (549 keV) agree with these energies and the cross sections for the transitions fit the signature of this band. Level 12 at 682 keV has the energy expected for the $\frac{11}{2}^-$ member of this rotational band.

4. $\frac{7}{2}$+[633]

The predicted signature of this band is not very definitive, composed only of a large cross-section transition to the $I=\frac{13}{2}$ level and a much smaller one to the $I=\frac{9}{2}$ level. In studies of energy levels of ^{243}Am populated by the α decay of ^{247}Bk and β decay of ^{243}Pu by Friedman *et al.*[14] the $\frac{7}{2}$+[633] band was identified at an energy 380 keV above the $\frac{5}{2}$+[642] band. These two bands appear to be strongly mixed by Coriolis forces and have an average rotational constant of 5.8 keV. The transitions to levels 13 (732 keV) and 14 (822 keV) fit the predicted signature of the $I=\frac{11}{2}$ and $\frac{13}{2}$ levels of this $\frac{7}{2}$+[633] band provided that the same coupling effects occur as for the $\frac{5}{2}$+[642] band; this assignment implies a rotational constant of 6.9 keV for this band and an average rotational constant of 5.7 keV for the $\frac{5}{2}$+[642] and $\frac{7}{2}$+[633] bands; also it implies that the $I=\frac{7}{2}$ state, not seen here, would be at 590 keV or 380 keV above the $\frac{5}{2}$+[642] state. For these reasons we are assigning these levels with confidence level C.

5. $\frac{1}{2}$+[400]

In Ref. 12 levels at 623 and 653 keV were identified as the $I=\frac{1}{2}$ and $\frac{3}{2}$ levels of a $K^\pi=\frac{1}{2}$ band. We have observed levels at 625 and 653 keV excitation which have cross sections similar to a pair of levels in ^{249}Bk which we have assigned as the $\frac{1}{2}$+[400] orbital.

6. $\frac{7}{2}$-[514]

We have assigned level 20 at 1163 keV as the $I^\pi=\frac{9}{2}^-$ member of the rotational band $\frac{7}{2}$-[514]. Level 21 (1227 keV) is at roughly the right energy to be the $\frac{11}{2}^-$ member of this rotational band, but the intensity is considerably greater than we expect from the calculated cross section based on the experimental signature found in ^{249}Bk. Because of this discrepancy we assign this orbital with confidence level C.

C. Level assignments in ^{231}Pa

Many levels in ^{231}Pa have been found in radioactive decay studies.[15,16] The present reaction data validate most of these previous assignments as well as providing the basis for a number of new assignments. An energy level diagram which summarizes these results are given in Fig. 13.

1. $\frac{1}{2}$-[530]

The $I=\frac{1}{2}$, $\frac{3}{2}$, $\frac{5}{2}$, and $\frac{7}{2}$ levels of this band were identified as being at 9.3, 0.0, 77.8, and 58.5 keV, respectively, by Browne and Asaro in studies of the decay of ^{231}Th and ^{235}Np as quoted in Ref. 15. Levels 0, 1, 2, and 3 are at these energies and the cross sections for populating these states fit the predicted signature for this band. The $I=\frac{11}{2}$ level of this band should be at 175 keV and level 7 at 172 keV is close to this energy. The cross section for populating the $I=\frac{11}{2}$ level should be about $\frac{1}{4}$ of that for populating the $I=\frac{7}{2}$ level, and the measured ratio of the cross sections of the transition to state 7 to that of state 2 is 0.29. Therefore, state 7 is assigned to the $I=\frac{11}{2}$ level of this band. The $\frac{9}{2}$ level should have about the same cross section as the $\frac{11}{2}$ level, but would be obscured by the large peak at 189 keV.

2. $\frac{3}{2}$+[651]

In Ref. 15 levels at 84.2, 102.2, 103, and 113 keV were assigned to the $I=\frac{5}{2}$, $\frac{3}{2}$, $\frac{7}{2}$, and $\frac{9}{2}$ levels, respectively, of the $\frac{3}{2}$+[651] band. The anomalous energy of the $I=\frac{3}{2}$ level was ascribed to a shift in the other rotational levels of the band due to strong Coriolis forces, especially due to coupling with the $\frac{5}{2}$+[642] band at 183.4 keV and the other $N=6$ states. We have duplicated these Coriolis force calculations and agree that the anomalous position of the $I=\frac{3}{2}$ state can be accounted for this way. The calculations also predict that the transfer

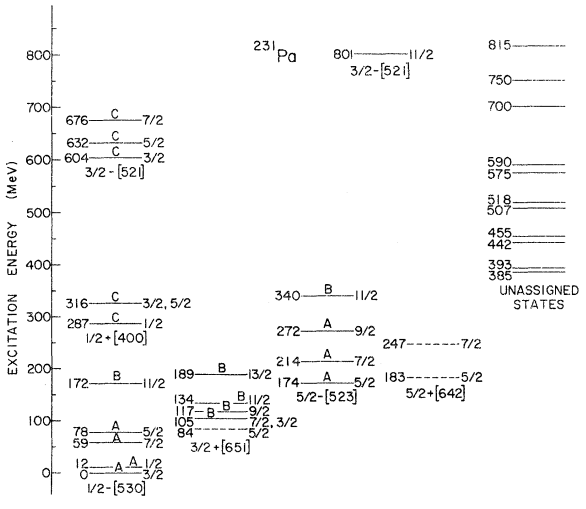

FIG. 13. Energy level diagram for ^{231}Pa. See caption of Fig. 10 for further description.

TABLE V. Parameters used to compute spectroscopic factors with the single-particle rotational model. Many of these parameters were found with the search code BANDFIT.

		^{249}Bk			^{241}Am			^{231}Pa		
Level No.	Orbital	E_0 (keV)	A (keV)	a	E_0 (keV)	A (keV)	a	E_0 (keV)	A (keV)	a
1	$\frac{9}{2}$+[624]	1081	6.0							
2	$\frac{7}{2}$−[514]	692	6.0		1109	6.0				
3	$\frac{7}{2}$+[633]	0	5.097		587	6.393				
4	$\frac{3}{2}$−[521]	12	6.72		473	6.821		602	5.802	
5	$\frac{5}{2}$+[642]	−389	5.015		−208	4.881		143	4.70	
6	$\frac{5}{2}$−[523]	−533	6.0		0	5.883		174	6.139	
7	$\frac{1}{2}$−[530]	−569	6.0	−1.90	−652	6.0	−1.90	8.3	6.717	−1.37
8	$\frac{3}{2}$+[651]							−104	5.488	
9	$\frac{1}{2}$+[400]	−377	6.71	0.749	−623					
10	$\frac{1}{2}$+[660]							−650	6.0	6.68
	rms deviation (keV)									
	Even parity		2.3			0.8			4.2	
	Odd parity		1.7			0.2			0.8	

cross section to the $I=\frac{13}{2}$ state will be very large; indeed equal to the sum of the strengths of the unmixed transitions to the $I=\frac{13}{2}$ levels of the $\frac{3}{2}$+[651] and $\frac{5}{2}$+[642] bands. Level 8 at 189 keV has about the correct energy for the $I=\frac{13}{2}$ level of the $\frac{3}{2}$+[651] band and has about the predicted cross section for the level. Consequently level 8 is assigned to this band but with confidence level B since its assignment is dependent on the accuracy of the Coriolis mixing calculations.

3. $\frac{5}{2}$−[523]

In Ref. 15 the β^- decay of ^{231}Th was seen to populate a $K=\frac{5}{2}$ rotational band with the $I=\frac{5}{2}$ level at 174.1 keV and $I=\frac{7}{2}$ level at 218.2 keV. This band was assigned as being the $\frac{5}{2}$−[523] state. This assignment indicates a rotational constant of 6.3 keV for this band which leads to a prediction of 274 keV for the $I=\frac{9}{2}$ level. Level 10 at 272 keV has the correct cross section for the transition to the $I=\frac{9}{2}$ level of this band. Levels 9 and 10 are therefore assigned as the $I=\frac{7}{2}$ and $\frac{9}{2}$ levels of this band. Part of the peak at level 7 (172 keV) may be due to the transition to the $I=\frac{5}{2}$ level but this should have a low cross section and should account for only a part of the observed strength of level 7. Level 13 at 340 keV has the correct energy and cross section for the transition to the $I=\frac{11}{2}$ level and is assigned to it.

4. $\frac{1}{2}$+[400]

The energy separation and cross section of the transitions to the levels at 287 and 316 keV resemble the signatures observed in the other nuclei for the state called $\frac{1}{2}$+[400]. In addition, an analysis of data by Freedman *et al.*[17] on the decay of ^{231}Th shows that a doublet at 318 and 320 keV in ^{231}Pa decays by γ cascades which have relative intensities consistent with the assignment of the 318- and 320-keV states as $I^\pi=\frac{5}{2}^+$ and $\frac{3}{2}^+$, respectively. However, it must be noted that these are not the only assignments which can satisfy the restrictions set by these relative intensities. Browne and Asaro[18,15] have identified the $\frac{1}{2}$+[400] state at an energy of 169 keV in ^{233}Pa with a spacing of 32 keV between the $I=\frac{1}{2}$ and $\frac{3}{2}$ states. Because of this and the consistency with the decay scheme data, we feel that these states can be assigned with a B confidence level.

5. $\frac{3}{2}$−[521]

This rotational band has been seen in ^{241}Am and ^{249}Bk where it is identified in radioactive decay studies. It was also observed by Elze and Huizenga in studies of proton transfer reactions to states in ^{237}Np. Levels 20, 21, and 22 fit the rotational spacings and signatures for the $I=\frac{3}{2}$, $\frac{5}{2}$, and $\frac{7}{2}$ levels, respectively, of this band and are assigned to those levels. However, we have only

TABLE VI. Reduction factors for Coriolis matrix elements.

Matrix-element indices [a]		^{249}Bk	^{241}Am	^{231}Pa
1	3	0.30		
2	6	0.30	0.25	
3	5	0.38	0.55	
4	6	0.80	0.84	0.75
4	7	0.88	0.41	0.60
5	8			0.81
8	9			0.56

[a] These indices refer to orbitals named and numbered in Table V.

given this assignment a confidence level of C due to the nonspecificity of the signature of this state.

D. Spectroscopic factors

A comparison of the observed differential cross sections with differential cross sections predicted by the single-particle rotational model was made in terms of the spectroscopic factor. Observed spectroscopic factors were extracted from the data with the formula obtained by rearranging Eq. (1), i.e.,

$$S_J^{\alpha} = (d\sigma_J^{\alpha}/d\Omega)/(2J+1)\theta_J^{\mathrm{DW}} \ . \tag{5}$$

The single-particle transfer cross section θ_J^{DW} was computed with a DWBA code as described in Sec. II.

Theoretical spectroscopic factors were calculated with the assumption of the single-particle rotational model including Coriolis mixing and pairing effects. A search code called BANDFIT[19] was used to find many of the model parameters by trying to fit the measured energies of the levels. The orbital and spin assignments made in Secs. IV A, IV B, and IV C were assumed.

The final parameters used in the calculations are listed in Table V. Some of these parameters were found by the search code when the data on excitation energies were sufficient. The spectroscopic factors were computed with Eq. (4) corrected for Coriolis mixing after a satisfactory energy fit was found. Nilsson wave functions were used instead of the more accurate deformed wave functions shown in Table I. Coriolis matrix elements were also calculated from Nilsson wave functions. Deformation parameter $\beta_2 = 0.25$ and $\kappa = 0.05$ were used. For $N = 5$ (6) orbits, the param-

TABLE VII. Spectroscopic factors for levels in ^{249}Bk.

Orbital	I	Excitation energy (keV) Reaction	Decay	Fitted	S_J (expt) (α,t)	$(^3\mathrm{He},d)$	S_J (theory) With mixing	Without mixing
$\frac{7}{2}^+[633]$	$\frac{9}{2}$	43 ± 3 [a]	41.80	42.67	0.20 ± 0.02 [b]	0.12 ± 0.02 [b]	0.0044	0.0037
	$\frac{11}{2}$		93.70	94.88				
	$\frac{13}{2}$	155 ± 1	155.80	156.65	0.58 ± 0.04	0.22 ± 0.02	0.080	0.068
	$\frac{15}{2}$		229.30	228.03				
$\frac{3}{2}-[521]$	$\frac{3}{2}$	7 ± 3	8.8	9.73	0.12 ± 0.02	0.076 ± 0.02	0.031	0.027
	$\frac{5}{2}$	43 ± 3 [a]	39.6	40.38			0.004	0.004
	$\frac{7}{2}$	83	82.6	81.68	0.55 ± 0.03	0.18 ± 0.02	0.127	0.111
	$\frac{9}{2}$	130 ± 3	137.7	138.34	<0.13	0.109 ± 0.04	0.011	0.009
	$\frac{11}{2}$	199 ± 3	204.6	200.46	0.05 ± 0.02	0.05 ± 0.02	0.010	0.007
	$\frac{13}{2}$		283.2	285.90				
$\frac{1}{2}+[400]$	$\frac{1}{2}$	377 ± 2	377.8		0.48 ± 0.04	0.11 ± 0.02	0.20	0.20
	$\frac{3}{2}$	413 ± 2			0.15 ± 0.02	0.050 ± 0.01	0.032	0.032
$\frac{1}{2}-[514]$	$\frac{9}{2}$	750 ± 1			1.30 ± 0.1	0.48 ± 0.03		0.13
$\frac{9}{2}+[624]$	$\frac{13}{2}$	1229 ± 2			0.34 ± 0.03	0.15 ± 0.02		0.13

[a] Unresolved doublet.

[b] Assumption has been made that the contribution from the $\frac{5}{2}-$ level of $\frac{3}{2}-[521]$ band is negligible.

TABLE VIII. Spectroscopic factors for levels in ^{241}Am.

Orbital	I	Excitation energy (keV) Reaction	Decay	Fitted	S_J (expt) (α,t)	S_J (theory) With mixing	Without mixing
$\frac{5}{2}$−[523]	$\frac{7}{2}$		41.17	40.90			
	$\frac{9}{2}$	95	93.40	93.57	0.66 ±0.05	0.098	0.092
	$\frac{11}{2}$	158 ± 2		157.91	0.027 ± 0.004	0.0018	0.0019
$\frac{5}{2}$+[642]	$\frac{5}{2}$		207.4	207.87			
	$\frac{7}{2}$	235 ± 5	237	237.01	0.037 ± 0.02	0.0001	0.0001
	$\frac{9}{2}$	272 ± 2	275	275.07	0.070 ± 0.01	0.006	0.0042
	$\frac{11}{2}$	323 ± 4	324	322.35	0.084 ± 0.02	0.0007	0.0004
	$\frac{13}{2}$	380 ± 1	378	379.09	0.35 ±0.02	0.074	0.040
$\frac{3}{2}$−[521]	$\frac{3}{2}$	475 ± 4	471.81	471.62	0.11 ±0.05		0.039
	$\frac{5}{2}$	504 ± 3	504.45	504.82	0.14 ±0.05		0.0053
	$\frac{7}{2}$	549 ± 1		548.84	0.60 ±0.05		0.17
$\frac{7}{2}$+[633]	$\frac{11}{2}$	732 ± 4		732.09		0.0010	0.0014
	$\frac{13}{2}$	822 ± 4		821.92	0.24 ±0.03	0.081	0.116

TABLE IX. Spectroscopic factors for levels in ^{231}Pa.

Orbital	I	Excitation energy (keV) Reaction	Decay	Fitted	S_J (expt) (α,t)	S_J (theory) With mixing	Without mixing
$\frac{1}{2}$−[530]	$\frac{3}{2}$	0	0	0	0.17 ±0.02	0.066	0.063
	$\frac{1}{2}$	12 ± 4	9.3	8.62	0.17 ±0.03	0.015	0.015
	$\frac{7}{2}$	59 ± 1	58.5	57.58	0.15 ±0.01	0.080	0.064
	$\frac{5}{2}$	78 ± 2	77.8	77.44	0.085 ± 0.02	0.0007	0.0005
	$\frac{11}{2}$	172 ± 3			0.063 ± 0.02	0.008	
$\frac{3}{2}$+[651]	$\frac{3}{2}$, $\frac{7}{2}$	105 ± 3	102.3, 101.4	102.7, 94.0			
	$\frac{9}{2}$	117 ± 4	111.6	112.65	0.072 ± 0.02	0.019	0.008
	$\frac{11}{2}$	134 ± 5		144.74	0.040 ± 0.02	0.0011	0.0003
	$\frac{13}{2}$	189 ± 1		182.97	0.43 ±0.04	0.15	0.05
$\frac{5}{2}$−[523]	$\frac{5}{2}$		174.1	173.88			
	$\frac{7}{2}$	214 ± 2	218.3	216.81	0.081 ± 0.02	0.003	0.004
	$\frac{9}{2}$	272 ± 1		272.01	0.73 ±0.05	0.128	0.128
	$\frac{11}{2}$	340 ± 3			0.031 ± 0.01		0.003
$\frac{3}{2}$−[521]	$\frac{3}{2}$	604 ± 1		602.47			
	$\frac{5}{2}$	632 ± 3		632.90			
	$\frac{7}{2}$	676 ± 2		675.04	0.24 ±0.03		0.15

eter $\mu = 0.70$ (0.62) was used. To obtain a fit to the energies, it was necessary to multiply the Coriolis matrix elements by the reduction factors shown in Table VI. The amount of the reduction was obtained from a procedure suggested by Casten *et al.*[20] Estimated values of the pairing emptiness factor U^2 were used, since more precise values would affect the mixed spectroscopic factor only slightly.

The quality of the various fits is indicated by the rms deviations which are shown in Table V. These range from 0.2 to 4.2 keV. The worst case is the even parity levels of ^{231}Pa. In this nucleus the $K^\pi = \frac{3}{2}^+$ and $\frac{5}{2}^+$ bands are strongly influenced by another band, possibly $\frac{1}{2}+[660]$, since the rotational parameters for the $K=\frac{3}{2}$ and $\frac{5}{2}$ bands are unusually low. An estimated energy for the $\frac{1}{2}+[660]$ was used and this may be responsible for the poor fit.

The mixed and unmixed spectroscopic factors calculated with the single-particle rotational model are listed in Tables VII–IX, together with the spectroscopic factors extracted from the measured cross sections with Eq. (5). The agreement between theory and experiment or between the (α, t) and $(^3\mathrm{He}, d)$ experiment is not good. There is a rough correlation between many of the theoretical and experimental spectroscopic factors but in some cases there is strong disagreement. We note that better consistency between the (α, t) and $(^3\mathrm{He}, d)$ results could have been obtained by arbitrarily increasing the (α, t) normalization factor $N=46$ by a factor of 2 or 3.

The measured spectroscopic factors in most cases are larger than the theoretical ones by a factor of 2 to 10 or more. It is not clear how significant this result is since the optical-model parameters used in the DWBA calculations are only estimated parameters. However, the discrepancy in spectroscopic factors is similar to that found[21] for sub-Coulomb neutron transfer reactions on ^{238}U and ^{232}Th. Here the most likely explanation is that the simple theory used to calculate the form factor does not give the correct radial tail to the bound state wave function. Possibly such an effect occurs in the present case with the (α, t) and $(^3\mathrm{He}, d)$ reactions on actinide targets.

The DWBA calculations were performed with a code in which the zero-range approximation is made. It would be interesting to do these same calculations with an exact finite-range DWBA code such as the ones developed by DeVries[22] and by Tamura and Low.[23] Perhaps some of the discrepancies in absolute spectroscopic factors and the problems with the $(\alpha, t)/(^3\mathrm{He}, d)$ cross section ratios discussed below would be explained.

E. Cross section ratio $d\sigma(\alpha,t)/d\sigma(^3\mathrm{He},d)$

The l dependence of the cross section ratio $d\sigma(\alpha, t)/d\sigma(^3\mathrm{He}, d)$ has been used previously to make level assignments in the actinide region[1,24] and in the rare earth region.[25] We, therefore, tried to analyze our data on ^{249}Bk with the help of this technique. The results are disappointing.

In Fig. 14 are plotted some of measured cross section ratios from Table II together with theoretical ratios computed with the DWBA code. A strong dependence on the reaction Q value is apparent in the computed curves. An arbitrary normalization factor of $N=120$ was used for the (α, t) reaction to bring the calculated ratios into better agreement with the data. The $(^3\mathrm{He}, d)$ normalization factor was kept at its theoretical value of 4.42. In Fig. 14 the four solid circles correspond to levels well identified in the radioactive decay studies. The known l values are marked above each circle. The agreement between measured and computed ratio is not good. The ratios for the 83- and 155-keV levels, known to be $l=3$ and 6, respectively, are not as different as the computed curves indicate.

Open circles in Fig. 14 indicate levels assigned in the present work. The circles corresponding to $l=1$, 5, and 6 levels agree well with the theoretical ratios. Two experimental ratios at 377 and 413 keV are not labeled with l values. These belong to those levels which we have assigned to the $\frac{1}{2}+[400]$ state and on the basis of this assignment would have the values of $l=0$ and 2. The measured ratio of 3.7 ± 0.6 for the 377-keV level

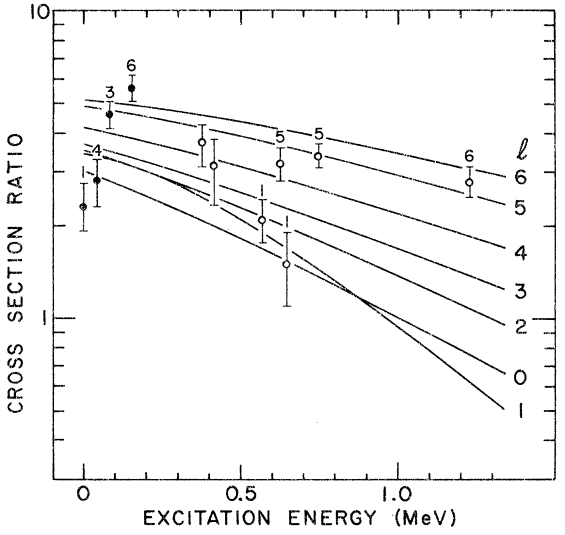

FIG. 14. Cross section ratio $d\sigma(\alpha,t)/d\sigma(^3\mathrm{He},d)$. The curves were computed with DW theory under the conditions given in Sec. II.

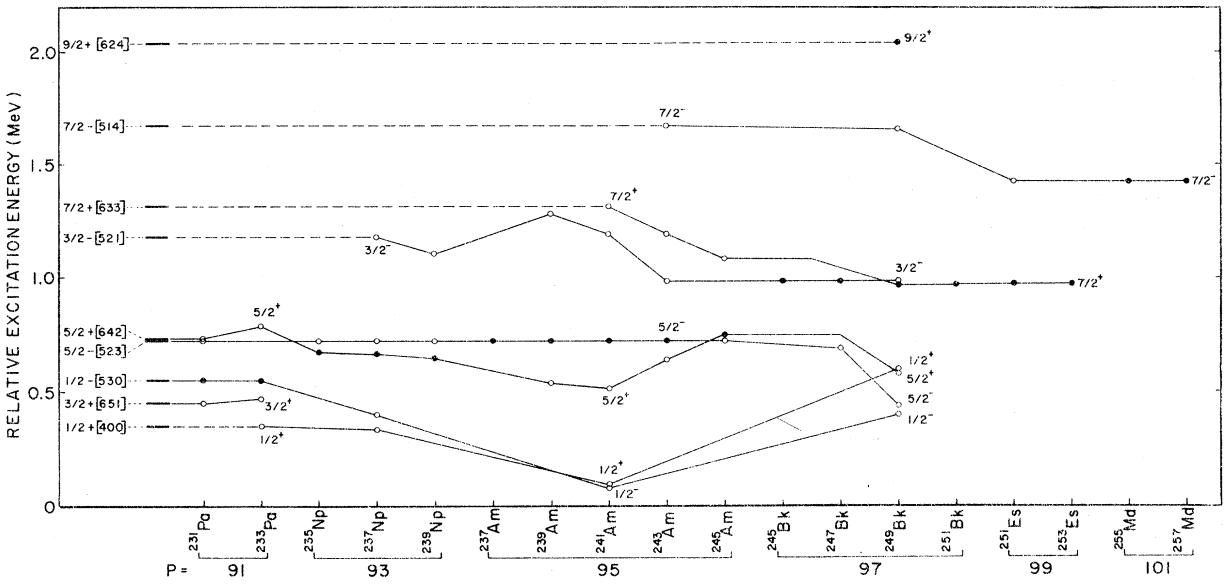

FIG. 15. Bandhead energies of single-proton excited states in odd-proton actinide nuclei. Somewhat arbitrary displacements have been introduced to bring all energies onto a common scale. Each state is labeled according to its asymptotic numbers.

is in serious disagreement with a computed ratio of 2.1. However, this discrepancy should not be taken seriously since the $l=3$ and $l=4$ points are also not in good agreement. We do not understand the source of these disagreements.

F. Systematics of the observed single-particle energies

The experimentally observed bandhead energies of the single-particle states in ^{249}Bk, ^{241}Am, and ^{231}Pa are displayed in Fig. 15 together with most of the known bandhead energies for single-proton states in other actinide nuclei. Arbitrary displacements have been introduced between nuclei of differing Z to bring all energies onto a common scale of excitation energy. The ground states are indicated by solid circles. The successive filling of orbitals as the proton number is increased is readily apparent.

G. Extracted proton single-particle energies

In Figs. 16–18, we present the proton single-particle spectra extracted from the experimental data on ^{249}Bk, ^{241}Am, and ^{231}Pa. The extracted spectra are calculated assuming a pairing force residual interaction, with a strength

$$G = 30/A \text{ MeV}$$

and 30 doubly degenerate levels in the system being considered. The calculations are done using previously described methods.[26] In these same figures we also present single-particle energies calculated with the momentum dependent Woods-Saxon potential discussed in Sec. II. The magnitudes of the β_2, β_4, and β_6 deformations are given above each calculated spectrum.

The agreement between the energy spectra calculated with our potential and the energy spectra extracted from the experimental data is remark-

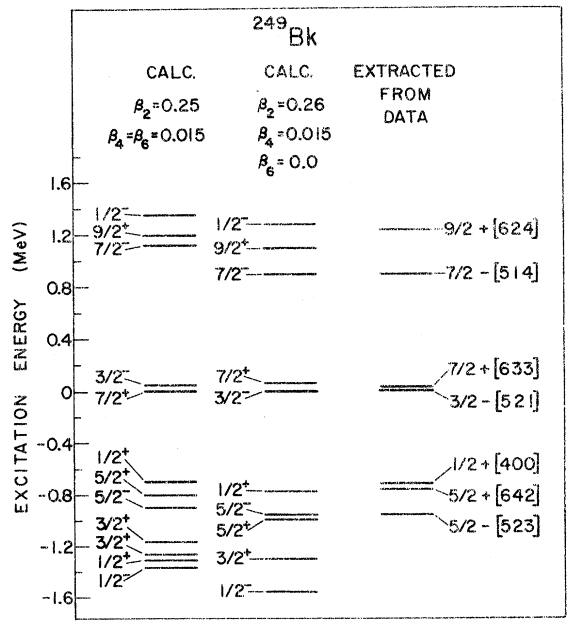

FIG. 16. Proton single-particle spectra extracted from the data on ^{249}Bk and compared to calculated spectra. As discussed in the text, the extraction procedure removes the pairing effects.

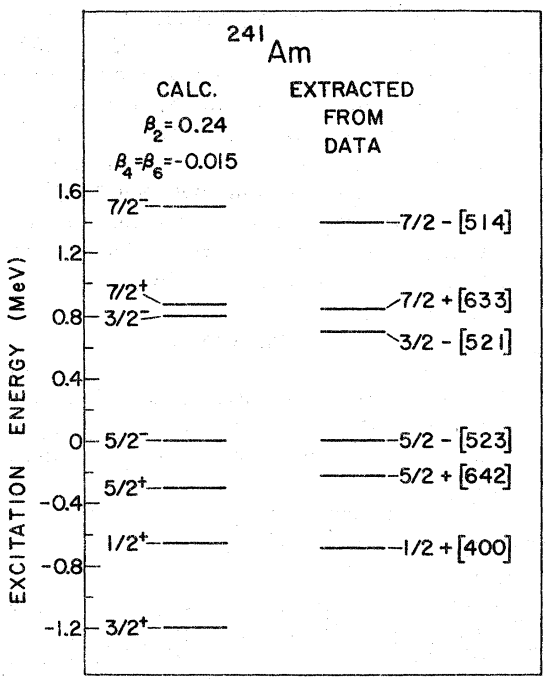

FIG. 17. Proton single-particle spectra extracted from the data on ^{241}Am and compared to calculated spectra.

ably good for ^{249}Bk and ^{241}Am, but rather poor for ^{231}Pa. Certain spacings in the calculated spectra are quite sensitive to the magnitudes of the different potential deformation multipoles. This is particularly true for the three orbitals $\frac{5}{2}+[642]$, $\frac{5}{2}-[523]$, and $\frac{1}{2}+[400]$. The positions of these

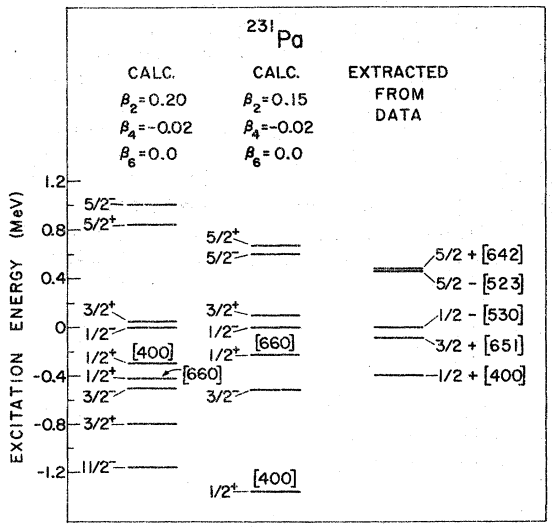

FIG. 18. Proton single-particle spectra extracted from the data on ^{231}Pa and compared to calculated spectra.

orbitals in the extracted spectra of ^{241}Am and ^{249}Bk fix the magnitudes of β_2, β_4, and β_6 rather well for these two nuclides. It is significant that the deformations we deduce from the proton spectra are quite similar to the deformations that we have deduced previously from our studies of a neutron single-particle spectra[4] in neighboring nuclei.

We have not included the $\frac{1}{2}-$ levels tentatively identified in ^{249}Bk at energies of 500 and 650 keV. Clearly, as noted above, these levels cannot be simply identified with the orbitals $\frac{1}{2}-[521]$ and $\frac{1}{2}-[530]$. With a pairing force interaction, we calculate that both of these pure configurations should be at ~1100 keV in ^{249}Bk. However, we note that these orbitals are of the $[k, \pm(k+1)]$ type[27] that are expected to have fairly large 0^+ particle-particle residual interaction matrix elements. There are fewer such orbital combinations for the actinide protons than there are for the actinide neutrons. Our most reasonable estimate of the matrix elements associated with these couples is

$$\overline{V}_{\frac{1}{2}-[521],\frac{1}{2}-[530];\,j,-j} \approx 0.5 \text{ G}.$$

Using a recently developed method,[27] we have calculated the single-particle excitation energy of the mixed $\frac{1}{2}-$ orbital including these 0^+ matrix elements. We find that the energy of one $\frac{1}{2}-$ configuration is lowered to 900 keV. However, this energy is extremely sensitive to the value of the average matrix element used. If we increase this matrix element to 0.7 G, i.e., by 24 keV, the energy of this state is lowered to 640 keV. This suggests that the anomalously low energy of one $\frac{1}{2}^-$ band could be accounted for by effects due to the nonpairing 0^+ particle-particle residual interactions. Gareev *et al.*[28] have calculated energy levels in ^{249}Bk and find that γ-vibrational and octupole-vibrational effects are also important in lowering the energies of the $\frac{1}{2}-$ configurations in ^{249}Bk. The two calculations are not directly comparable; however, it is clear that we learn very little directly about the single particle energy of the pure orbital $\frac{1}{2}-[521]$ in ^{249}Bk.

One reason that the $\frac{1}{2}-[521]$ single-particle energy is interesting is the fact that the major spherical component of the orbital $\frac{1}{2}-[521]$ is $f_{5/2}$. From this single-particle energy, we can deduce the $f_{7/2}$-$f_{5/2}$ splitting in the spherical proton single-particle spectrum. It is this splitting that has been postulated to give rise to shell effects at $Z=114$. In view of the fact that our potential gives such a good over-all fit to the remaining levels in ^{249}Bk, we feel that one can have considerable confidence in an estimate of this splitting at mass 250 by simply setting all deformations equal to

zero in our potential. We have carried out such a calculation and find the $f_{5/2}$-$f_{7/2}$ splitting is 2.3 MeV when calculated in this way. Extrapolating to heavier masses this gives an expected splitting of ~2.0 MeV for $f_{7/2}$-$f_{5/2}$ in the mass 300 region. This estimate is quite similar to one obtained by extrapolating from hole states the ^{208}Pb region. The advantage here is that we are now extrapolating over a mass interval that is one-half as large and this should be more reliable.

As we have noted above, we are not able to find single-particle potential parameters that give a good fit to the extracted spectrum of ^{231}Pa. Nevertheless, the potential does give good level orderings. The apparent β_2 deformation is quite small here—slightly less than 0.20. The indications concerning the β_4 and β_6 deformations are somewhat contradictory. The near degeneracy of the orbitals $\frac{5}{2}+[642]$ and $\frac{5}{2}-[523]$ argues for a β_4 of ~ -0.02 as in the figure. On the other hand, the measured decoupling parameter of -1.4 for the orbital $\frac{1}{2}-[530]$ argues for β_4 of ~ -0.04 or for β_6 of ~ -0.02. The effect of either of such changes is to further increase the spacing between the $\frac{5}{2}+[642]$ and the $\frac{1}{2}-[530]$ orbitals. A more complete calculation involving additional terms in the residual interaction appears to be in order here.

ACKNOWLEDGMENTS

We would like to acknowledge the aid of J. Lerner in preparing the isotopically separated targets and want to thank I. Ahmad for many helpful discussions.

*Work performed under the auspices of the U.S. Atomic Energy Commission.

[1]Th. W. Elze and J. R. Huizenga, Phys. Rev. C 1, 328 (1970).

[2]J. R. Erskine, G. Kyle, A. Friedman, and R. Chasman, Bull. Am. Phys. Soc. 17, 928 (1972).

[3]J. R. Erskine and G. Kyle, John H. Williams Laboratory of Nuclear Physics, University of Minnesota Annual Report, 1972 (unpublished), p. 97.

[4]T. H. Braid, R. R. Chasman, J. R. Erskine, and A. M. Friedman, Phys. Rev. C 1, 275 (1970); T. H. Braid, R. R. Chasman, J. R. Erskine, and A. M. Friedman, *ibid.* 4, 247 (1971); T. H. Braid, R. R. Chasman, J. R. Erskine, and A. M. Friedman, *ibid.* 6, 1374 (1972).

[5]P. D. Kunz, University of Colorado.

[6]R. H. Siemssen and J. R. Erskine, Phys. Rev. 146, 911 (1966).

[7]R. R. Chasman, Phys. Rev. C 3, 1803 (1971).

[8]J. E. Spencer and H. A. Enge, Nucl. Instrum. Methods 49, 181 (1967).

[9]P. Spink and J. R. Erskine, Argonne National Laboratory, Physics Division Informal Report No. PHY-1965B (unpublished); J. R. Comfort, Argonne National Laboratory, Physics Division Informal Report No. PHY-1970-B (unpublished).

[10]Y. A. Ellis and A. H. Wapstra, Nucl. Data B3(No. 2), 1 (1969), and references contained therein.

[11]R. W. Hoff, J. E. Evans, L. G. Mann, J. F. Wild, and R. W. Tougheed, Bull. Am. Phys. Soc. 16, 494 (1971).

[12]F. T. Porter, I. Ahmad, M. S. Freedman, J. Milsted, and A. M. Friedman, Phys. Rev. C 10, 803 (1974).

[13]Y. A. Ellis, Nucl. Data B6, 621 (1971), and references contained therein.

[14]A. M. Friedman, I. Ahmad, J. Milsted, and D. W. Engelkemeir, Nucl. Phys. A127, 33 (1969).

[15]E. Browne and F. Asaro, Phys. Rev. C 7, 2545 (1973).

[16]A. Artna-Cohen, Nucl. Data B6, 225 (1971), and references contained therein.

[17]M. S. Freedman, A. H. Jaffey, F. Wagner, Jr., and J. May, Phys. Rev. 89, 302 (1953).

[18]E. Browne and F. Asaro, University of California Radiation Laboratory Report No. UCRL-17989, 1968 (unpublished).

[19]This code was developed by J. R. Erskine and E. Sutter.

[20]R. F. Casten, P. Kleinheinz, P. J. Daly, and B. Elbek, Phys. Rev. C 3, 1271 (1971).

[21]J. R. Erskine, Phys. Rev. C 5, 959 (1972).

[22]R. M. DeVries, Phys. Rev. C 8, 951 (1973).

[23]T. Tamura and K. S. Low, Phys. Rev. Lett. 31, 1356 (1973).

[24]T. W. Elze and J. R. Huizenga, Nucl. Phys. A149, 585 (1970).

[25]See, for example, J. S. Boyno and J. R. Huizenga, Phys. Rev. C 6, 1411 (1972).

[26]R. R. Chasman, Phys. Rev. C 5, 29 (1972).

[27]R. R. Chasman, Phys. Rev. C 8, 1896 (1973).

[28]F. A. Gareev, C. P. Ivanova, L. A. Malov, and V. G. Soloviev, Dubna Report No. P4-5470, 1970 (unpublished).